ADVANCED ELECTRONIC MATERIALS
www.advelectronicmat.de

Dimensionality Dependent Plasticity in Halide Perovskite Artificial Synapses for Neuromorphic Computing

*Sung-Il Kim, Yeongjun Lee, Min-Ho Park, Gyeong-Tak Go, Young-Hoon Kim, Wentao Xu, Hyeon-Dong Lee, Hobeom Kim, Dae-Gyo Seo, Wanhee Lee, and Tae-Woo Lee**

The hysteretic behavior of organic–inorganic halide perovskites (OHPs) are exploited for application in neuromorphic electronics. Artificial synapses with 2D and quasi-2D perovskite are demonstrated that have a bulky organic cation (phenethylammonium (PEA)) to form structures of $(PEA)_2MA_{n-1}Pb_nBr_{3n+1}$. The OHP films have morphological properties that depend on their structure dimensionality (i.e., *n* value), and artificial synapses fabricated from them show synaptic responses such as short-term plasticity, paired-pulse facilitation, and long-term plasticity. The operation mechanism of OHP artificial synapses are also analyzed depending on the dimensionality and it is found that quasi-2D (n = 3–5) OHP artificial synapses show much longer retention than 2D and 3D OHP counterparts. The calculated energy consumption of a 2D OHP artificial synapse (≈0.7 f) per synaptic event) is comparable to that of biological synapses (1–10 f) per synaptic event). These OHP artificial synapses may enable development of neuromorphic electronics that use very little energy.

Neuromorphic computing emulates the functions of a brain and operates at low power, and is therefore becoming a core technology to demonstrate future artificial intelligence and to overcome the limitations of conventional structures.[1–3] To implement the neuromorphic system, various types of electronic devices have been developed based on phase-change memory,[1] resistive switching memory,[2] magnetoresistive memory,[3] atomic switches,[4] and synaptic functional transistors.[5,6] Although these devices could mimic the important properties of biological synapses and perform parallel operations, they require larger energy than a biological synapse. Therefore, development of an artificial synapse with energy consumption on the level of a biological synapse remains an open problem.

Organic–inorganic halide perovskite (OHPs) may provide a material to solve this problem, because of their low activation energy of ion migration. Moreover, various structural modulation of polycrystalline films is possible with facile solution processing so that organic parts in the OHPs can control the ion migration and electrical conduction. OHPs have an ABX_3 crystal structure; the A-site cation is located at the center of a BX_6 octahedral cage, and the B-site metal cation is surrounded by the six nearest-neighbor X-site halide anions.[7] OHPs have a significant hysteresis property that is caused by ion migration or space charges, or both, which may enable gradual modulation of conductance in OHP.[8]

Two-terminal artificial synapses based on 3D methylammonium (MA) lead halide perovskite ($MAPbX_3$, X = Br, I) films showed synaptic responses that are caused by ion migration in the OHP layer.[9,10] Ion migration in 3D OHP film is induced by relatively low activation energy and a low energy consumption of ≈20 fJ per synaptic event was achieved in the synaptic devices. However, the energy consumption could be further reduced to the energy level of biological synapses when the ion migration was controlled by engineering the structure of OHP films could be optimally done.

In this work, we introduce 2D and quasi-2D OHP films into artificial synapses to enable control of ion migration and resultant synaptic responses. For this purpose, we replaced the small MA ion with a bulky phenethylammonium (PEA) ion in their crystalline structures. To prepare 2D, quasi-2D, and 3D OHP films, we controlled the stoichiometric ratio of PEA and MA cations to induce self-assembly of a layered structure. This replacement of an MA cation with PEA cation suppresses ion migration in the out-of-plane direction of the OHP films.[11–13] Thereby, the activation energy E_A of ion migration is increased, so ion migration and excitatory postsynaptic current (EPSC) can be reduced. Also, energy consumption of the device is reduced to ≈0.7 fJ per synaptic event, which is comparable to that of biological synapses. Memory retention of artificial

S.-I. Kim, Dr. Y. Lee, Dr. M.-H. Park, G.-T. Go, Dr. Y.-H. Kim, Dr. W. Xu, H.-D. Lee, Dr. H. Kim, D.-G. Seo, W. Lee
Department of Materials Science and Engineering
Seoul National University (SNU)
1 Gwanak-ro, Gwanak-gu, Seoul 08826, Republic of Korea
Prof. T.-W. Lee
Department of Materials Science and Engineering
Nano Systems Institute (NSI)
Institute of Engineering Research
Research Institute of Advanced Materials
BK21 PLUS SNU Materials Division for Educating
Creative Global Leaders
Seoul National University (SNU)
1 Gwanak-ro, Gwanak-gu, Seoul 08826, Republic of Korea
E-mail: twlees@snu.ac.kr, taewlees@gmail.com
The ORCID identification number(s) for the author(s) of this article can be found under https://doi.org/10.1002/aelm.201900008.

DOI: 10.1002/aelm.201900008

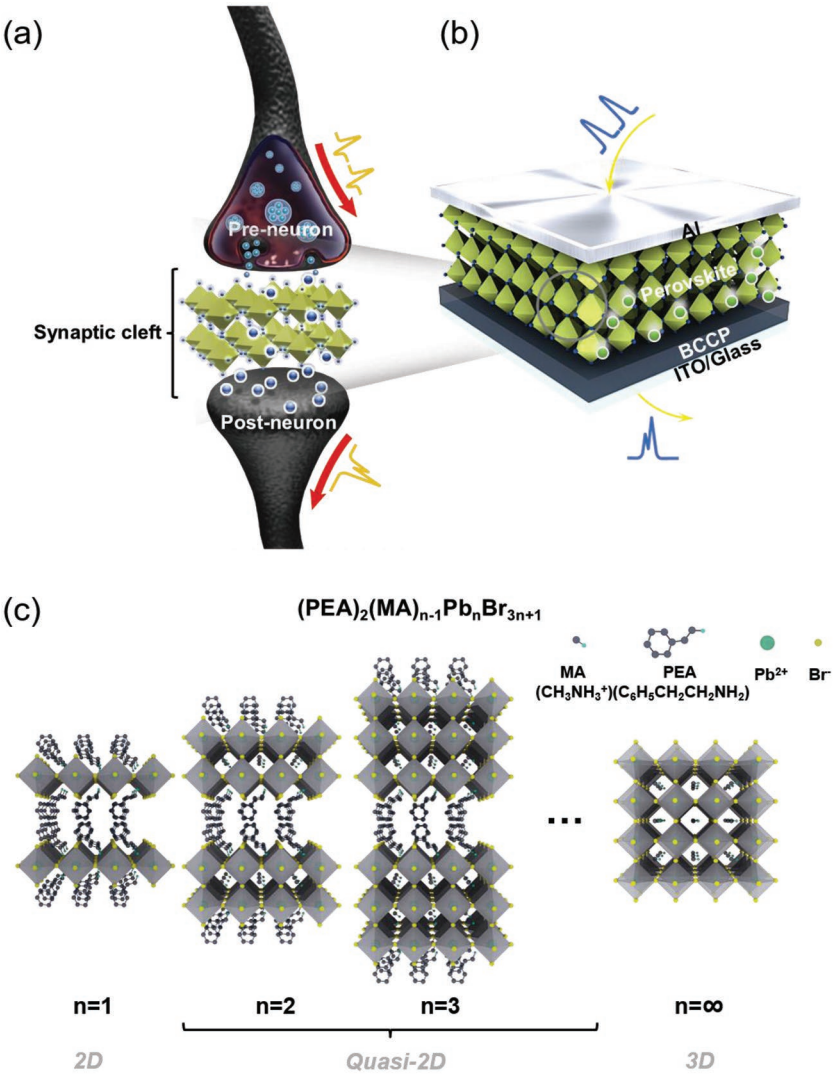

Figure 1. Schematics of perovskite artificial synapses and perovskite structure. a) Schematic illustration, b) device geometry of a perovskite artificial synapses, c) crystal structure of perovskite ($(PEA)_2(MA)_{n-1}Pb_nBr_{3n+1}$) with structural dimensionality.

synapse was controlled by adjusting the dimensionality of the perovskite structure. We quantified synaptic properties such as paired-pulse facilitation (PPF), short-term potentiation (STP), long-term potentiation (LTP), spike-frequency dependent plasticity (SFDP), spike-duration dependent plasticity (SDDP), spike-voltage dependent plasticity (SVDP), and spike-number dependent plasticity (SNDP). Furthermore, we simulated pattern recognition of handwritten digits with our perovskite artificial synapses to show promise for use in future neuromorphic computing devices.[14,15]

The OHP artificial synapses were fabricated with the two-terminal device structure of ITO (bottom electrode)/buffer-capped conducting polymer (BCCP)/OHP/Al (top electrode) (**Figure 1**a,b), where BCCP consists of poly(3,4-ethylenedioxythiophene)-poly(styrene sulfonate) (PEDOT:PSS) (Heraeus Clevios AI 4083) with a perfluorinated ionomer (PFI), tetrafluoroethylene-perfluoro-3,6-dioxa-4-methyl-7-octene-sulfonic acid copolymer (PEDOT:PSS:PFI = 1:2.5:11.2 (w:w:w)). The Al top electrode mimics the presynaptic membrane to which the presynaptic spike is applied, and the ITO bottom electrode mimics the postsynaptic membrane at which the postsynaptic current is read. A synaptic electrical spike applied to the top electrode induces ion migration and consequently modulates the conductance of the OHP thin films.[9] The BCCP layer blocks the formation of conductive filaments through the devices, so the devices do not have bi-stable states (Figure S1, Supporting Information).

OHP films with 2D, quasi-2D, and 3D structures were used as the active layers of artificial synapses. The configuration of OHP thin films could be defined by the number of $PbBr_6$ layers between PEA layers; this number depends on the ratio of MA and PEA cations, and the molecular formula of OHPs can be expressed as $(PEA)_2MA_{n-1}Pb_nBr_{3n+1}$. The structural dimensionality depends on the ratio.[16] For example, if $n = 1$, one $PbBr_6$ layer forms between the large organic ammonium layers, so 2D $(PEA)_2PbBr_4$ is achieved; if $n \geq 2$, two or a few $PbBr_6$ layers form between the large organic ammonium layers, so quasi-2D $(PEA)_2MA_{n-1}Pb_nBr_{3n+1}$ forms; and if $n = \infty$, 3D $MAPbBr_3$ forms (Figure 1c).

$(PEA)_2MA_{n-1}Pb_nBr_{3n+1}$ (n = 1–5, ∞) films were spin-coated on BCCP/ITO substrate in an N_2-filled glovebox. Toluene was used as an antisolvent for the nanocrystal-pinning (NCP) process (see the details in the Experimental Section and Figure S2, Supporting Information), so the thin films were pinhole-free with smooth surfaces (**Figures 2**a, S3 and S4, Supporting Information). As n increased, the bandgap of OHPs decreased,[11,16] so the films became yellowish. The films showed different photoluminescence (PL) under UV (365 nm) lamp excitation (Figure 2a). 2D $(PEA)_2PbBr_4$ ($n = 1$) emitted blue PL because of the strong quantum confinement in a very thin quantum well. Quasi-2D (n = 2–5) films emitted bright greenish PL due to cascade energy transfer (or energy funneling).[7] 3D $MAPbBr_3$ ($n = \infty$) showed no PL emission because the excitons have low exciton binding energy at room temperature, so they are mostly dissociated.[11]

In steady-state PL measurement, the structural relaxation of the crystal lattice increased the optical bandgap, so the lattice expansion in 2D $(PEA)_2PbBr_4$ film yielded a blue-shifted PL spectrum (Figure 2b and Table S1, Supporting Information).[17,18] In UV–vis absorption spectra, 2D $(PEA)_2PbBr_4$ and 3D $MAPbBr_3$ films showed absorption peaks near wavelengths λ = 401 and 525 nm, respectively. In contrast, the absorption peaks of quasi-2D perovskite films gradually red-shifted to λ = 401, 432, 450 nm (n = 2–5) as n increased because of different quantum and dielectric confinement effects;[7,11] and the absorption peaks at 401 and 432 nm

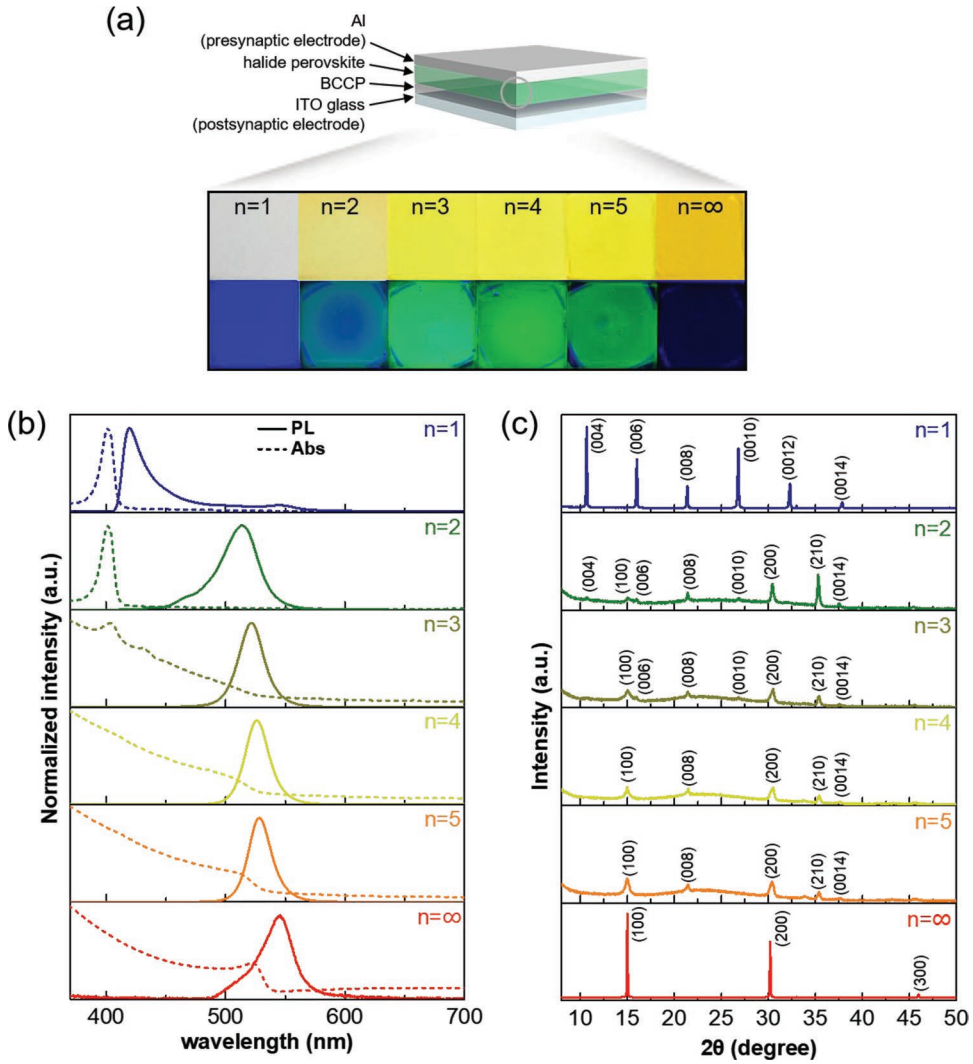

Figure 2. Optical analysis of perovskite films a) Schematic of perovskite thin-film on BCCP layer and ITO substrate (top) and photoluminescence under UV (365 nm) (bottom). b) UV–vis absorption and photoluminescence (PL) spectra and c) XRD spectra of $(PEA)_2(MA)_{n-1}Pb_nBr_{3n+1}$ film with structural dimensionality.

became strong because proportions of n = 1, 2 domains became dominant.[11]

The X-ray diffraction (XRD) patterns of the films showed a clear tendency of structural changes from 2D to 3D as n increased (Figure 2c).[11] For 2D $(PEA)_2PbBr_4$ ($n = 1$), (00l) reflections were dominant; this result is characteristic of an ordered layer structure in the out-of-plane direction of the 2D layers.[17] Quasi-2D perovskite films (n = 2–5) showed additional peaks depending on the number of layers. For 3D $MAPbBr_3$ ($n = \infty$), (h00) reflections were dominant.

Synaptic plasticity is involved in learning and memory by strengthening or weakening synaptic weight over time in response to synaptic activity.[19] In a biological synapse, excitatory postsynaptic response shows a temporary increase in synaptic weight due to the flow of ions to the postsynaptic membrane. Similarly, in our device, when a pulse was applied temporarily, the postsynaptic current was abruptly increased by voltage-induced ion migration, then gradually decayed over time due to back-diffusion of ions (**Figure 3**a). In quasi-2D perovskites, the large insulating PEA cations suppress charge transport so the conductivity decreases as the ratio of PEA increases, i.e., as n decreases.[11]

In a biological synapse, STP is a temporal modulation of synaptic strength; it is involved in associative learning, pattern recognition, and sound localization.[20,21] If stimuli are not sustained, the postsynaptic current quickly returns to the initial state within hundreds to thousands of milliseconds. In our artificial synapses, when negative presynaptic voltage pulses (–1 V) were applied, EPSC was induced by migration of bromide ions (Br^-), and yielded a temporary enhancement of the conductivity of OHP. After the voltage pulses were removed, migrated ions diffused back to the original position, so the film conductivity decreased and current was decayed.

PPF is a kind of STP in which the synaptic strength temporarily increases when paired-pulses are applied within a short interval Δt. Analogously, the synaptic weight of our artificial synapse

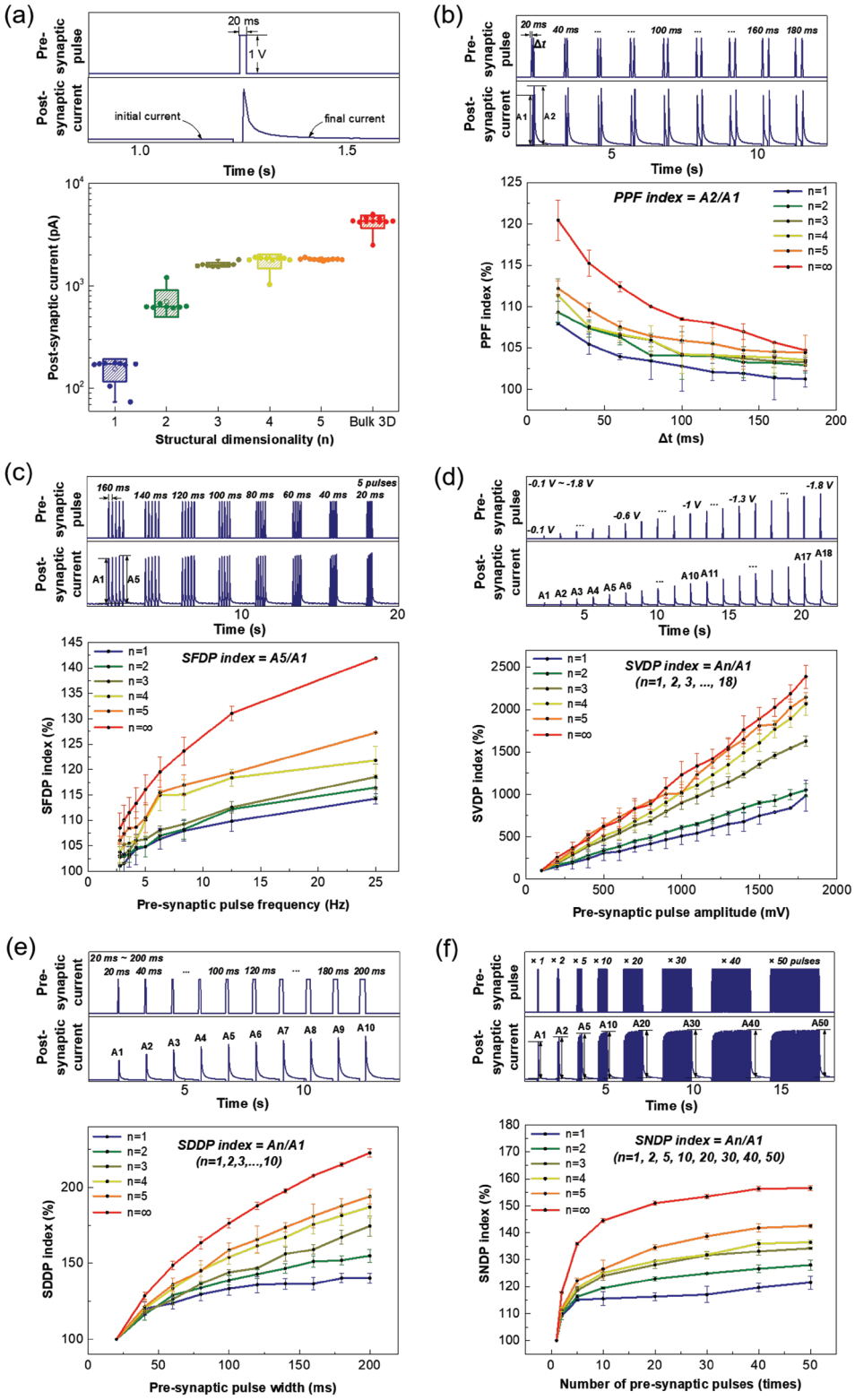

Figure 3. Spike-dependent plasticity in perovskite artificial synapses. a) Excitatory postsynaptic current (EPSC) of perovskite artificial synapses triggered by an applied external pulse, b) paired pulse facilitation (PPF) index (A2/A1) achieved by two successive pulses with various time interval $20 \leq \Delta t \leq 180$ ms, c) SFDP index (A5/A1) according to the spike frequency from 2.8 to 25 Hz (A1: 1st postsynaptic current, A5: 5th postsynaptic current), d) SVDP index (A*n*/A1) according to the spike voltage amplitude from –0.1 to –1.8 V (A*n*: *n*th postsynaptic current, $n = 1, 2, 3, ..., 18$), e) SDDP index (A*n*/A1) according to the spike duration from 20 to 200 ms ($n = 1, 2, 3, ..., 10$), and f) SNDP index (A*n*/A1) according to the number of spikes ($n = 1, 2, 5, 10, 20, 30, 40, 50$). Default spike voltage amplitude and duration were –1 V and 20 ms, respectively. The magnitude of read voltage was –0.01 V.

increased when two consecutive stimuli were applied (Figure 3b). The change in conductance of the OHP layer was dependent on Δt. PPF increased as Δt decreased from 180 to 20 ms, because back-diffusion of Br^- ions decreased as Δt was decreased; therefore, learning and memory are strengthened.

SFDP is considered to be an extended form of Hebbian learning, and is related to learning, associative memory, and forgetting.[22] Repeated synaptic spikes with various frequency (2.8 to 25 Hz) were applied to the artificial synapse (Figure 3c). EPSC increased as the spike frequency increased, because high-rate pulses increased ion migration and prevented back-diffusion of ions in the OHP when the pulse was removed.

SVDP, SDDP, and SNDP were also observed in our artificial synapse (Figure 3d–f and Figures S5, S6, and S7, Supporting Information). As the pulse magnitude (from –0.1 to –1.8 V), the pulse duration (from 20 to 200 ms), and the number of pulses (from 1 to 50) were increased, the number of Br^- that migrated increased, and the induced changes in conductivity of OHP increased, thereby EPSC increasing proportionally.

The multistore model proposed by Atkinson and Shiffrin suggests that human memory has three components: sensory memory, short-term memory, and long-term memory (**Figure 4**a).[23] If sensory stimuli are repeated frequently, short-term memory is converted to long-term memory. Similarly, we can induce the STP–LTP transition in our artificial synapses by applying several repeated stimuli (Figures 4b, and S8, Supporting Information). The memory decay curve in our artificial synapses is similar to the "forgetting curve" (Figures S7, S8 and S9, Supporting Information).[23] When 30 pulses were applied, the decay of memory retention fitted a power function $y = b \times t^{-m}$, where y is the synaptic weight, b is the fit constant for scaling, t is the time, and m is the power function rate.[22] As m decreases, the retention curve slowly decreases, i.e., the duration of memory increases.[23] Quasi-2D films with $n = 3, 4, 5$ have smaller m than 3D film, so quasi-2D films have longer retention than 3D film. The difference occurs because back-diffusion of migrated anions is hindered by the bulky PEA cations when the voltage is removed, so the increased current is maintained for a long time. However, in quasi-2D films with $n = 1, 2$, the large content of insulating PEA would prohibit ion migration seriously and allow only very small amount of ions to migrate when the voltage is applied, so it seems that the potentiated current retention is unnoticeable.

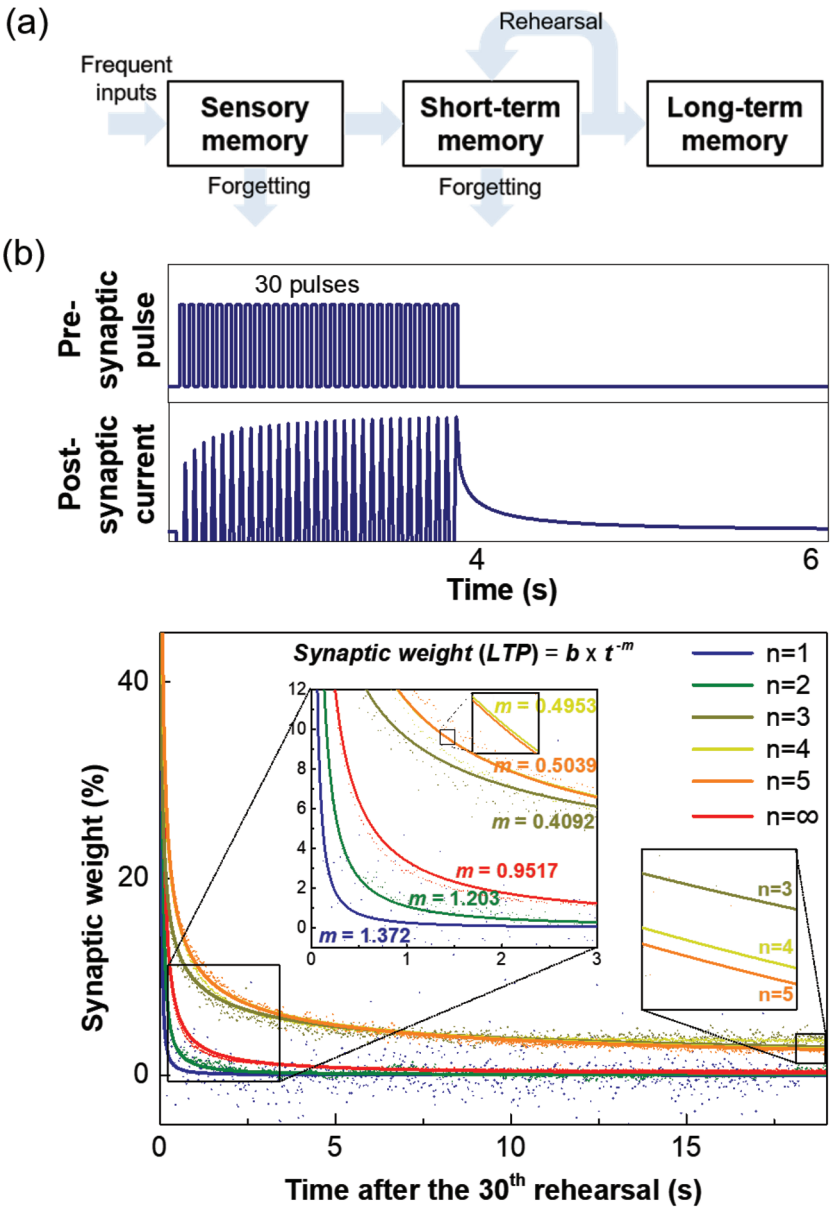

Figure 4. Long-term plasticity in perovskite artificial synapses. a) Multistore model of human memory proposed by Atkinson and Shiffrin, b) Current decay curves of perovskite synapses after the 30th rehearsal. Decay curves fitted as $y = b \times t^{-m}$, where y is synaptic weight, b is fit constant for scaling, t is time, and m is a power function rate. The magnitude of the applied pulses was –1 V (duration: 20 ms), and that of the read voltage was –0.1 V.

We hypothesize that the dimensionality of the OHP film affects the migration of ions in it. When voltage pulses are applied, ions migrate, and then when the voltage pulses are removed, the ions diffuse back into their original distribution.[9] In 3D films, ions are relatively free to move along defects such as grain boundaries (**Figure 5**a).[24] In contrast, in quasi-2D perovskites, the large insulating PEA cations are positioned between $PbBr_6$ layers (Figure 5a), so the PEA impede movement of halide ions and thereby increase the E_A of halide ion migration.[25] Therefore, as the amount of PEA increases (e.g., $n = 1, 2$), the migration of Br^- ions is significantly suppressed. As n of

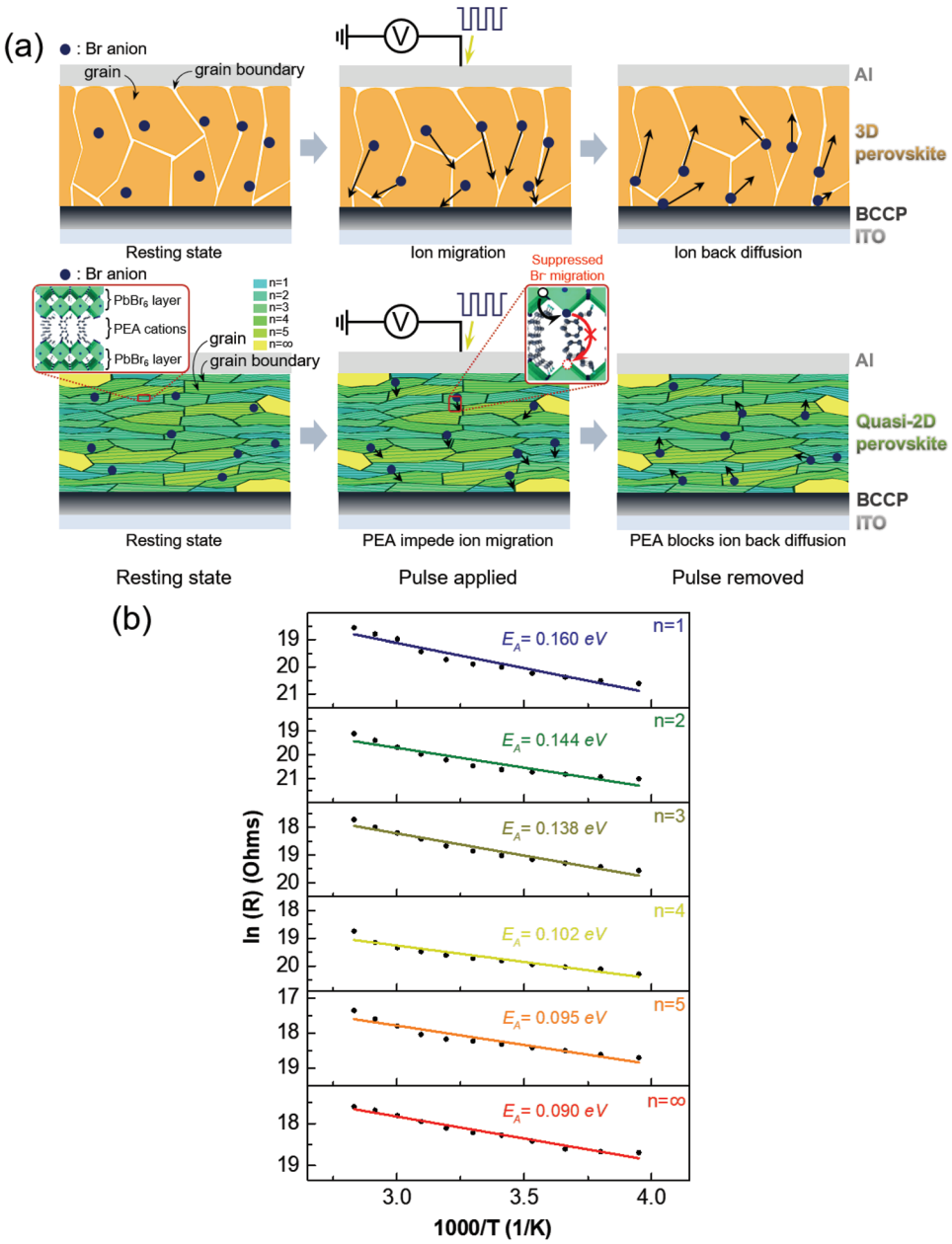

Figure 5. Ion migration in perovskite artificial synapses. a) Schematics of ion migration in the 3D (top) and quasi-2D (bottom) perovskite layers. b) Arrhenius plot of resistance in perovskite artificial synapses with structural dimensionality. Activation energy was calculated by fitting the linear region.

quasi-2D perovskites increases (n = 3–5), the ease of Br^- ion migration increases compared to low-dimensional quasi-2D (n = 1, 2) when driving voltage is applied, but when the voltage is removed, the PEA impedes ion back-diffusion in quasi-2D perovskites.

We compared E_A in all OHP films to support our explanation (Figure 5b). Br^- ions have the smallest E_A in the 3D $MAPbBr_3$ film (**Table 1**),[26–28] so when applied voltage is small (–1 V), most of the ions that migrate in the OHP films may be Br^-.[9] In Arrhenius plots of OHP films by the equation of $\ln R(T) = \ln R_0 + E_A/(kT)$, where R is the resistance, R_0 is the pre-exponential factor, k is the Boltzmann constant, and T is the absolute temperature. The magnitude of E_A decreased as n increased

Table 1. Activation energies for ion migration in halide perovskites.

Defect	Defect notation	E_A [eV]	Reference
$CH_3NH_3^+$ (MA^+)	V_{MA}'	0.46–0.56	[26]
		0.84	[27]
		0.80–1.13	[28]
Pb^{2+}	V_{Pb}''	0.80	[26]
		2.31	[27]
		1.35–1.80	[28]
Br^-	$V_{Br}^{\bullet}$	0.09–0.16	[26]
		0.2–0.46	[28]

Table 2. Constant of the memory retention curve and activation energies for ion vacancy migration in halide perovskite artificial synapses.

Configuration [*n*]	Fit constant [*b*]	Power function rate [*m*]	E_A [eV]
1	0.002795	1.372	0.160
2	0.01096	1.205	0.144
3	0.09594	0.4092	0.138
4	0.1142	0.4953	0.102
5	0.1145	0.5039	0.095
∞	0.03129	0.9517	0.090

(Figure 5b and **Table 2**). Under the bias, ion migration may cause not only conductance enhancement and but also ion concentration gradient across the OHP film which induces band bending at the interface and facilitates charge injection into OHP films. As PEA concentration increased, ion migration is suppressed due to bulky PEA, thus resistance of the film is increased and charge injection would be hindered. Therefore, we deduce that PEA in quasi-2D OHP films has a major effect on activation of ion transport and on back-diffusion of ions in OHP layers, and consequently can control synaptic plasticity of perovskite synapses.

A biological synapse has high energy efficiency (1–10 fJ per synaptic event).[22] The energy consumption of the artificial synapses is calculated as $E = PIt$, where P [V] is the magnitude of voltage pulse, I [A] is postsynaptic current, and t [s] is pulse width.[29] Postsynaptic current is linearly dependent on the device dimension, so the calculated energy consumption also has a linear dependency on the device dimension (**Figure 6**a).[10] The magnitude of postsynaptic current was smallest in the 2D perovskite synapse; its calculated energy consumption was also lowest when voltage amplitude and pulse width were fixed (Figure 6a). The calculated energy consumption of 2D perovskite synapse (≈18 fJ per synaptic event for a device of 250 µm × 250 µm at voltage pulse = –1 V and read voltage = –0.01 V) is comparable to the energy consumed by biological synapses. Also, we further economized on energy consumption of the device by decreasing the magnitude of voltage pulse (≈0.7 fJ per synaptic event at voltage pulse = –0.02 V and read voltage = –0.01 V) (Figure S10, Supporting Information). Compared with the recently reported energy consumption of fabricated artificial synapses (Figure 6b and Table S2, Supporting Information),[5,12,13,22,29–40] our OHP artificial synapses show much higher energy efficiency despite having larger dimension. This energy efficiency would be a great advantage in neuromorphic computing system.

We further demonstrated synaptic potentiation/depression characteristics, and simulated pattern classification of our perovskite synapse with $PEA_2MA_2Pb_3Br_{10}$ (n = 3) (Figure S11, Supporting Information). By applying 20 negative spikes (–1 V, 20 ms) and 20 positive spikes (1 V, 20 ms), we gradually controlled the conductance of the perovskite layer; the distinct conductance states were almost linearly adjusted (Figure S11a, Supporting Information). Also, we simulated classification of our perovskite synapse for an 8 × 8 pixel and a 28 × 28 pixel images of handwritten digits; the training results showed accuracy of 91.26% and 84.24%, respectively (Figure S11b,c, Supporting Information). These results of our perovskite synapse show promise for use in future neuromorphic computing devices.

In conclusion, we reported halide perovskite artificial synapses that have energy consumption that is as low as that of a biological synapse. Artificial synapses composed of 2D, quasi-2D, and 3D OHP films with various structural dimensionality emulated EPSC, PPF, STP, and LTP. The quasi-2D OHP artificial synapses showed increased long-term retention over 3D OHP synapse, and 2D OHP artificial synapse had femtojoule-level energy consumption (≈0.7 fJ per synaptic event), which is similar to those of biological synapses (1–10 fJ per synaptic event). Energy consumption of the device can be further decreased to much lower than that of the biological synapse by using state-of-art photolithography to minimize the device size. We showed the structural dimensionality–dependent operational behaviors of perovskite artificial synapses which can be correlated with the calculated activation energy for ion migration of perovskite films with different dimensionalities. We expect that our approach will have applications in perovskite artificial synapses to demonstrate energy-efficient neuromorphic computing.

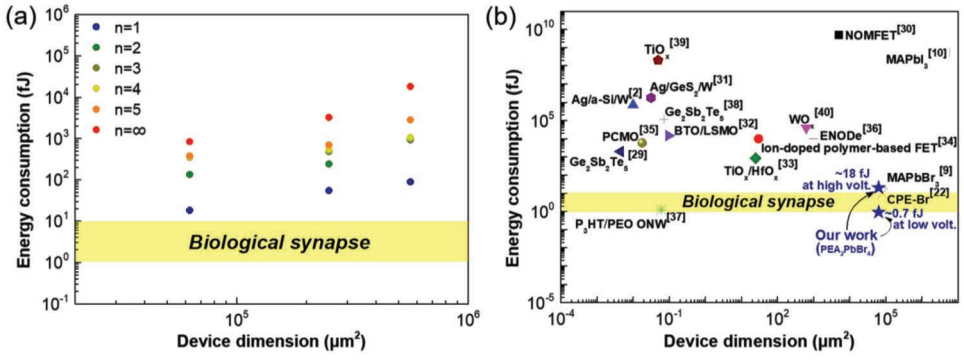

Figure 6. Energy efficiency of perovskite artificial synapses. Energy consumption of devices a) with structural dimensionality (device dimensions 6.25 × 10⁴ µm², 2.5 × 10⁵ µm², 5.625 × 10⁵ µm²), and b) compared with previously reported devices. Energy consumption was calculated as $E = PIt$ where (P [V] is the magnitude of pulse amplitude, I [A] is postsynaptic current level, and t [s] is pulse width).

Supporting Information

Supporting Information is available from the Wiley Online Library or from the author.

Acknowledgements

S.-I.K. and Y.L. contributed equally to this work. This work was supported by the National Research Foundation of Korea (NRF) grant funded by the Korea government (Ministry of Science, ICT & Future Planning) (NRF-2016R1A3B1908431). This work was also supported by the Center for Advanced Soft-Electronics funded by the Ministry of Science, ICT, and Future Planning as Global Frontier Project (2013M3A6A5073175), and Creative-Pioneering Researchers Program through Seoul National University (SNU).

Conflict of Interest

The authors declare no conflict of interest.

Keywords

neuromorphic electronics, neuromorphic memory, perovskite synapses, quasi-2D perovskite, synaptic devices

Received: January 2, 2019
Revised: February 24, 2019
Published online: March 28, 2019

[1] D. Kuzum, R. G. D. Jeyasingh, B. Lee, H.-S. P. Wong, *Nano Lett.* **2012**, *12*, 2179.
[2] S. H. Jo, T. Chang, I. Ebong, B. B. Bhadviya, P. Mazumder, W. Lu, *Nano Lett.* **2010**, *10*, 1297.
[3] M. Gajek, J. J. Nowak, J. Z. Sun, P. L. Trouilloud, E. J. O'Sullivan, D. W. Abraham, M. C. Gaidis, G. Hu, S. Brown, Y. Zhu, R. P. Robertazzi, W. J. Gallagher, D. C. Worledge, *Appl. Phys. Lett.* **2012**, *100*, 132408.
[4] T. Hasegawa, T. Ohno, K. Terabe, T. Tsuruoka, T. Nakayama, J. K. Cimzewski, M. Aono, *Adv. Mater.* **2010**, *22*, 1831.
[5] Y. Lee, J. Y. Oh, W. Xu, O. Kim, T. R. Kim, J. Kang, Y. Kim, D. Son, J. B.-H. Tok, M. J. Park, Z. Bao, T.-W. Lee, *Sci. Adv.* **2018**, *4*, eaat7387.
[6] Y. Kim, A. Chortos, W. Xu, Y. Liu, J. Y. Oh, D. Son, J. Kang, A. M. Foudeh, C. Zhu, Y. Lee, S. Niu, J. Liu, R. Pfattner, Z. Bao, T.-W. Lee, *Science* **2018**, *360*, 998.
[7] Y.-H. Kim, H. Cho, T.-W. Lee, *Proc. Natl. Acad. Sci. USA* **2016**, *113*, 11694.
[8] J. M. Frost, K. T. Butler, F. Brivio, C. H. Hendon, M. Van Schilfgaarde, A. Walsh, *Nano Lett.* **2014**, *14*, 2584.
[9] W. Xu, H. Cho, Y.-H. Kim, Y.-T. Kim, C. Wolf, C.-G. Park, T.-W. Lee, *Adv. Mater.* **2016**, *28*, 5916.
[10] Z. Xiao, J. Huang, *Adv. Electron. Mater.* **2016**, *2*, 1600100.
[11] J. Byun, H. Cho, C. Wolf, M. Jang, A. Sadhanala, R. H. Friend, H. Yang, T.-W. Lee, *Adv. Mater.* **2016**, *28*, 7515.
[12] X. Xiao, J. Dai, Y. Fang, J. Zhao, X. Zheng, S. Tang, P. N. Rudd, X. C. Zeng, J. Huang, *ACS Energy Lett.* **2018**, *3*, 684.
[13] J. Y. Seo, J. Choi, H. S. Kim, J. Kim, J. M. Yang, C. Cuhadar, J. S. Han, S. J. Kim, D. Lee, H. W. Jang, N. G. Park, *Nanoscale* **2017**, *9*, 15278.
[14] P. Yao, H. Wu, B. Gao, S. B. Eryilmaz, X. Huang, W. Zhang, Q. Zhang, N. Deng, L. Shi, H. P. Wong, H. Qian, *Nat. Commun.* **2017**, *8*, 15199.
[15] T. Wang, Z. He, H. Liu, L. Chen, H. Zhu, Q. Sun, S. Ding, *ACS Appl. Mater. Interfaces* **2018**, *10*, 37345.
[16] K. Tanaka, T. Kondo, *Sci. Technol. Adv. Mater.* **2003**, *4*, 599.
[17] L. Dou, A. B. Wong, Y. Yu, M. Lai, N. Kornienko, S. W. Eaton, A. Fu, C. G. Bischak, J. Ma, T. Ding, N. S. Ginsberg, L.-W. Wang, A. P. Alivisatos, P. Yang, *Science* **2015**, *349*, 1518.
[18] L.-C. Chen, Z.-L. Tseng, J.-K. Huang, C.-C. Chen, S. Chang, *Coatings* **2016**, *6*, 53.
[19] T. Chang, S. H. Jo, W. Lu, *ACS Nano* **2011**, *5*, 7669.
[20] L. F. Abbott, W. G. Regehr, *Nature* **2004**, *431*, 796.
[21] P. A. Merolla, J. V. Arthur, R. Alvarez-Icaza, A. S. Cassidy, J. Sawada, F. Akopyan, B. L. Jackson, N. Imam, C. Guo, Y. Nakamura, B. Brezzo, I. Vo, S. K. Esser, R. Appuswamy, B. Taba, A. Amir, M. D. Flickner, W. P. Risk, R. Manohar, D. S. Modha, *Science* **2014**, *345*, 668.
[22] W. Xu, T. L. Nguyen, Y. T. Kim, C. Wolf, R. Pfattner, J. Lopez, B. G. Chae, S. Il Kim, M. Y. Lee, E. Y. Shin, Y. Y. Noh, J. H. Oh, H. Hwang, C. G. Park, H. Y. Woo, T. W. Lee, *Nano Energy* **2018**, *48*, 575.
[23] T. Ohno, T. Hasegawa, T. Tsuruoka, K. Terabe, J. K. Gimzewski, M. Aono, *Nat. Mater.* **2011**, *10*, 591.
[24] L. Malavasi, C. A. J. Fisher, M. S. Islam, *Chem. Soc. Rev.* **2010**, *39*, 4370.
[25] Y. Chen, Y. Sun, J. Peng, J. Tang, K. Zheng, Z. Liang, *Adv. Mater.* **2018**, *30*, 1.
[26] J. M. Azpiroz, E. Mosconi, J. Bisquert, F. De Angelis, *Energy Environ. Sci.* **2015**, *8*, 2118.
[27] C. Eames, J. M. Frost, P. R. F. Barnes, B. C. O'Regan, A. Walsh, M. S. Islam, *Nat. Commun.* **2015**, *6*, 2.
[28] S. Meloni, T. Moehl, W. Tress, M. Franckevičius, M. Saliba, Y. H. Lee, P. Gao, M. K. Nazeeruddin, S. M. Zakeeruddin, U. Rothlisberger, M. Graetzel, *Nat. Commun.* **2016**, *7*, 10334.
[29] D. Kuzum, S. Yu, H.-S. Wong, *Nanotechnology* **2013**, *24*, 382001.
[30] F. Alibart, S. Pleutin, O. Bichler, C. Gamrat, T. Serrano-Gotarredona, B. Linares-Barranco, D. Vuillaume, *Adv. Funct. Mater.* **2012**, *22*, 609.
[31] M. Suri, O. Bichler, D. Querlioz, G. Palma, E. Vianello, D. Vuillaume, C. Gamrat, B. DeSalvo, in *2012 Int. Electron Devices Meet.*, IEEE, **2012**, pp. 10.3.1–10.3.4.
[32] A. Chanthbouala, A. Crassous, V. Garcia, K. Bouzehouane, S. Fusil, X. Moya, J. Allibe, B. Dlubak, J. Grollier, S. Xavier, C. Deranlot, A. Moshar, R. Proksch, N. D. Mathur, M. Bibes, A. Barthélémy, *Nat. Nanotechnol.* **2012**, *7*, 101.
[33] S. Yu, B. Gao, Z. Fang, H. Yu, J. Kang, H.-S. P. Wong, in *2012 Int. Electron Devices Meet.*, IEEE, **2012**, pp. 10.4.1–10.4.4.
[34] Q. Lai, L. Zhang, Z. Li, W. F. Stickle, R. S. Williams, Y. Chen, *Appl. Phys. Lett.* **2009**, *95*, 213503.
[35] S. Park, M. Chu, J. Kim, J. Noh, M. Jeon, B. H. Lee, H. Hwang, B. Lee, B. G. Lee, *Sci. Rep.* **2015**, *5*, 10123.
[36] Y. van de Burgt, E. Lubberman, E. J. Fuller, S. T. Keene, G. C. Faria, S. Agarwal, M. J. Marinella, A. A. Talin, A. Salleo, *Nat. Mater.* **2017**, *16*, 414.
[37] W. Xu, S. Min, H. Hwang, T. Lee, *Sci. Adv.* **2016**, *2*, e1501326.
[38] M. Suri, O. Bichler, D. Querlioz, B. Traoré, O. Cueto, L. Perniola, V. Sousa, D. Vuillaume, C. Gamrat, B. DeSalvo, *J. Appl. Phys.* **2012**, *112*, 054904.
[39] K. Seo, I. Kim, S. Jung, M. Jo, S. Park, J. Park, J. Shin, K. P. Biju, J. Kong, K. Lee, B. Lee, H. Hwang, *Nanotechnology* **2011**, *22*, 254023.
[40] R. Yang, K. Terabe, G. Liu, T. Tsuruoka, T. Hasegawa, J. K. Gimzewski, M. Aono, *ACS Nano* **2012**, *6*, 9515.